Journal of Inorganic Biochemistry 241 (2023) 112145

Contents lists available at ScienceDirect

Journal of Inorganic Biochemistry

journal homepage: www.elsevier.com/locate/jinorgbio

Iridium(III) complexes inhibit the proliferation and migration of BEL-7402 cells through the PI3K/AKT/mTOR signaling pathway

Jing Chen [a], Haimei Liu [a], Yichuan Chen [a], Huiyan Hu [a], Chunxia Huang [a], Yi Wang [a], Lijuan Liang [a], Yunjun Liu [a,b,*]

[a] School of Pharmacy, Guangdong Pharmaceutical University, Guangzhou 510006, PR China
[b] Guangdong Provincial Key Laboratory of Advanced Drug Delivery, Guangdong Provincial Engineering Center of Topical Precise Drug Delivery System, Guangdong Pharmaceutical University, Guangzhou, 510006, PR China

ARTICLE INFO

Keywords:
Iridium(III) complex
Apoptosis
Autophagy
ROS
Immunogenic cell death

ABSTRACT

Iridium(III) complexes are largely studied as anti-cancer complexes due to their excellent anti-cancer activity. In this article, two new iridium(III) complexes $[Ir(piq)_2(THPIP)]PF_6$ (THPIP = 2,4-di-tert-butyl-6-(1*H*-imidazo[4,5-f][1,10]phenanthrolin-2-yl)phenol, piq = deprotonated 1-phenylisoquinoline) (**Ir1**) and $[Ir(bzq)_2(THPIP)]PF_6$ (bzq = deprotonated benzo[*h*]quinolone) (**Ir2**) were synthesized. 3-(4,5-dimethylthiazol-2-yl)-2,5-diphenyltetrazolium bromide (MTT) assays showed that complex **Ir1** exhibits moderate activity ($IC_{50} = 29.9 \pm 4.6$ μM) and **Ir2** shows high cytotoxicity ($IC_{50} = 9.8 \pm 1.8$ μM) against BEL-7402 cells. Further studies on the mechanism showed that **Ir1** and **Ir2** induced apoptosis by changing the mitochondrial membrane potential, Ca^{2+} release, ROS accumulation, and cell cycle arrest at the S phase. The complexes can effectively inhibit cell colony formation and migration. The expression of B-cell lymphoma-2 (Bcl-2) family proteins, PI3K (phosphatidylinositol 3-kinase), AKT (protein kinase B), mTOR (mammalian target of rapamycin), and p-mTOR was studied by immunoblotting. Complexes **Ir1** and **Ir2** downregulated the expression of anti-apoptotic protein Bcl-2 and increased the expression of autophagy-related proteins of Beclin-1 and LC3-II. Further experiments showed that the complexes inhibited the production of glutathione (GSH) and increased the amounts of malondialdehyde (MDA). Fluorescence of HMGB1 was significantly increased. We also investigated the effect of the complexes on the expression of genes using RNA-sequence analysis, we further calculated the lowest binding energies between the complexes and proteins using molecular docking. Taken together, the above results indicated that complexes **Ir1** and **Ir2** induce apoptosis in BEL-7402 cells through a ROS-mediated mitochondrial dysfunction and inhibition of the PI3K/AKT/mTOR signaling pathway.

Abbreviations: A549, human lung cancer; AKT, protein kinase B; BAX, Bcl-2-Associated X; BCA, Bicinchoninic acid; Bcl-2, B-cell lymphoma-2; BEL-7402, (human hepatocellular carcinoma); BH3, The Bcl-2 Homology Domain 3; Bzq, deprotonated benzo[*h*]quinolone; CCCP, Carbonyl cyanide 3-chlorophenylhydrazone; CRT, calmodulin; DAMPs, damage-associated molecular patterns; DAPI, 4′,6-diamidino-2-phenylin-dole; DCF, 2′,7′-Dichlorofluorescein; DCFH-DA, 2′,7′ dichlorofluorescein diacetate; DMEM, dulbecco's modified eagle medium; DMSO, Dimethyl sulfoxide; ECL, enhanced chemiluminescence; FAK, Focal adhesion kinase; FBS, Fetal bovine serum; Fluo-3 AM, Fluo-3-pentaacetoxy-methyl ester; GSH, glutathione; HeLa, human cervical carcinoma; HepG2, human hepatocellular carcinoma; HMGB1, high mobility group box 1; HSP, heat shock protein; IC_{50}, half maximal inhibitory concentration; ICD, immunogenic cell death; JC-1, 5,5′,6,6′-tetrachloro-1,1′,3,3′-tetraethyl-benzimidazolylcarbocyanine iodide; LC3, microtubule-associated protein 1 light chain 3 alpha; LGA, Lamarckian genetic algorithm; LC3-I, a cytosolic form of LC3; LC3-II, LC3-phosphatidylethanolamine conjugate; LO2, liver cell line; MDA, malondialdehyde; MDC, monodansylcadaverine; MMP, mitochondrial membrane potential; M-TOR, mammalian target of rapamycin; MTT, 3-(4,5-dimethylthiazol-2-yl)-2,5-diphenyltetrazolium bromide; PARP, poly ADP-ribose polymerase; PBS, phosphate buffer saline; PI, propidium iodide; PI3K, phosphatidylinositol 3-kinase; Piq, deprotonated 1-phenylisoquinoline; PVDF, polyvinylidene fluoride; RIPA, Radio-Immunoprecipitation Assay; RNA-seq, RNA sequencing; ROS, Reactive Oxygen Species; RPMI, Roswell Park Memorial Institute; SDS-PAGE, sodium dodecyl sulfate polyacrylamide gel electrophoresis; SOD, superoxide dismutase; THPIP, 2,4-di-tert-butyl-6-(1H-imidazo[4,5-f][1,10]phenanthrolin-2-yl)phenol; TMS, tetramethylsilane; VEGF, vascular endothlial growth factor..

* Corresponding author.
E-mail address: lyjche@gdpu.edu.cn (Y. Liu).

https://doi.org/10.1016/j.jinorgbio.2023.112145
Received 23 November 2022; Received in revised form 11 January 2023; Accepted 20 January 2023
Available online 23 January 2023

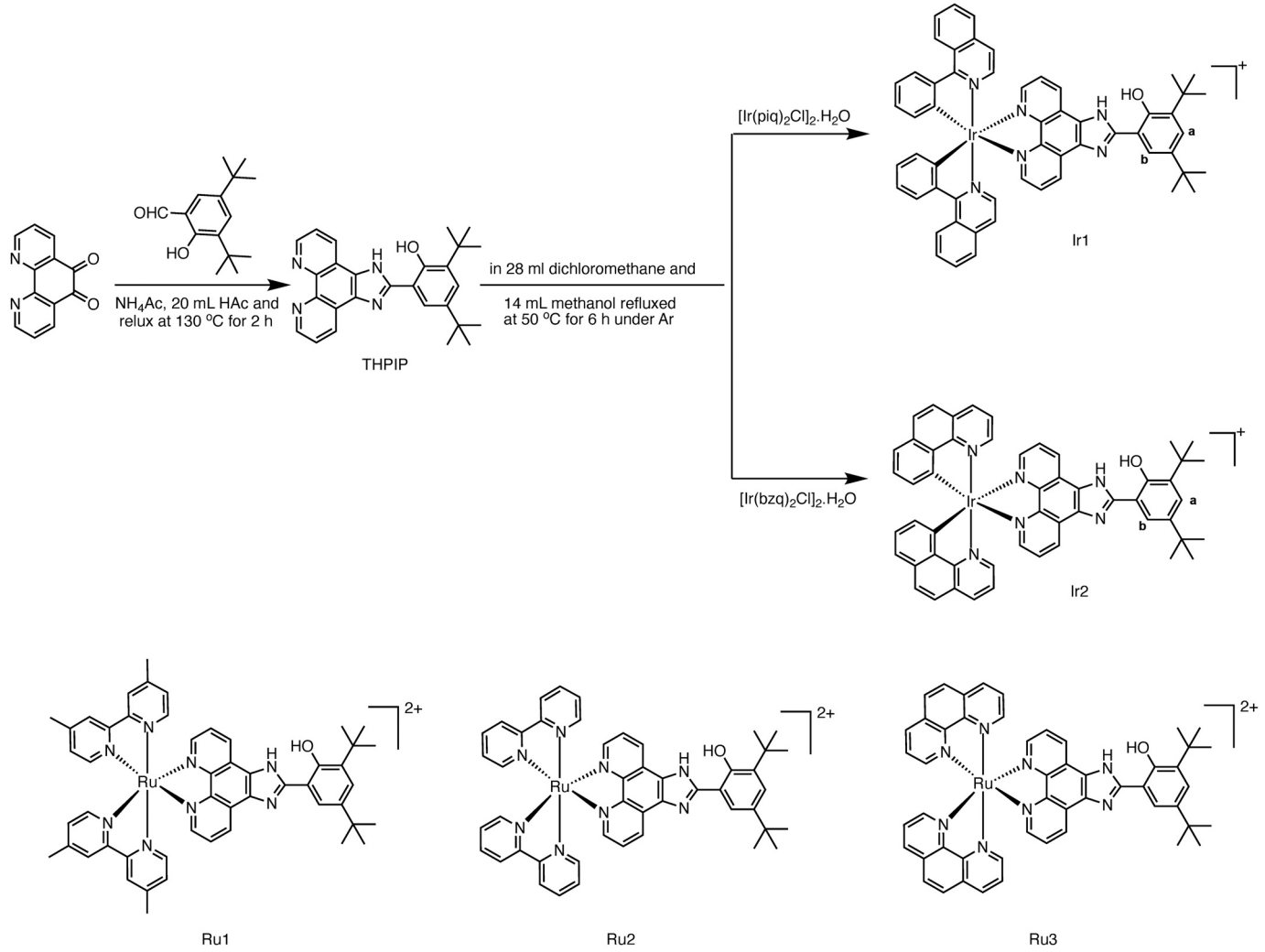

Scheme 1. Synthetic route of **THPIP**, complexes **Ir1**, **Ir2** and structures of **Ru1**, **Ru2** and **Ru3**.

1. Introduction

Hepatocellular carcinoma is one of the deadliest forms of cancer and the second cancer death worldwide, with approximately 800,000 new patients each year, making it a global health challenge [1–3]. Although therapies such as surgery, chemotherapy, and immunotherapy have been used in the clinical management of hepatocellular carcinoma, the prognosis for patients with hepatocellular carcinoma remains unfavorable [4]. The drug resistance and severe side effects of platinum drugs have limited their clinical use, which prompts researchers to develop other metal compounds such as iridium(III) complexes as potential tumor imaging and therapeutic agents [5–10]. Cao et al. reported a series of Ir(III) complexes with bipyridyl ligands that significantly reduced mitochondrial membrane potential (MMP), oxygen consumption rate, and ATP production [11]. Thomas et al. synthesized a series of guanidino and thiourea iridium compounds with high cytotoxicity based on the 2-aminobenzimidazole unit, offering new potential therapeutic avenues for ovarian cancer [12]. Chen et al. reported four iridium(III) complexes to induce both autophagy and apoptosis and eventually lead to A549 cells death [13].

It has been suggested that anticancer drugs may damage mitochondria by increasing the permeability of the outer mitochondrial membrane, which in turn affects the mitochondrial membrane potential ($\Delta\Psi_m$) [14]. And the defective mitochondrial function is involved in the induction of cancer cell death [15]. Huang et al. reported a light-induced intracellular redox imbalance and alteration of mitochondrial membrane potential leading to necrosis and apoptosis of tumor cells by Ir(III) complexes [16]. In addition, autophagy and apoptosis are two important physiological activities that control cell survival and death, both of which are anti-cancer pathways [17]. It was reported that two Ir(III)-β-caroline complexes were identified as potent inducers of autophagy [18]. Our previous work reported that Ir(III) complexes can inhibit cell proliferation by inducing apoptosis and autophagy [19].

Ruthenium(II) complexes (**Ru1**, **Ru2**, **Ru3**, Scheme 1) with THPIP (2,4-di-tert-butyl-6-(1*H*-imidazo[4,5-f][1,10]phenanthrolin-2-yl) phenol) as ligand showed high inhibitory activity against A549 lung cancer cell and moderate cytotoxic activity toward BEL-7402 cells [20]. To explore the difference in the anticancer effect of the classical Werner Ru(II) complexes and organometallic Ir(III) complexes, in this paper, we used iridium(III) in place of Ru(II), and synthesized two new organometallic iridium(III) complexes: $[Ir(piq)_2(THPIP)(PF_6)$ (piq = deprotonated 1-phenylisoquinoline) (**Ir1**) and $[Ir(bzq)_2(THPIP)]PF_6$ (bzq = deprotonated benzo[*h*]quinolone) (**Ir2**) (Scheme 1), these complexes were characterized by fluorescence, UV–Vis, HRMS, ^{1}H NMR and ^{13}C NMR spectra. Their anticancer activity was examined by cytotoxicity in vitro, apoptosis, mitochondrial localization, mitochondrial membrane potential, intracellular Ca^{2+} levels, reactive oxygen species (ROS), cellular uptake, cell cloning, cell migration, cell cycle arrest and immunoblotting.

2. Experimental

2.1. Materials and methods

All reagents and solvents are commercially purchased, and they were used without further purification. $IrCl_3{\cdot}3H_2O$ was obtained from Kunming Boren Precious Metals Co., Ltd. 1-phenylisoquinoline (piq) and benzo[*h*]quinolone (bzq) were purchased from Beijing HWRK Chem Co., Ltd. 2-hydroxy-3,5-di-tert-butylbenzaldehyde was purchased from Acros Organics, Inc. A549 (human lung cancer), HepG2 (human hepatocellular carcinoma), BEL-7402 (human hepatocellular carcinoma), HeLa (human cervical carcinoma), and human normal liver LO2 cells were obtained from the cell center of Sun Yat-Sen University (Guangzhou, China). Fetal bovine serum (FBS) and Duchenne Modified Eagle Medium (DMEM) were obtained from Gibco. Fluorescent dyes and related assay kits were purchased from Beyotime Biotechnology (Shang Hai). 3-(4,5-dimethylthiazol-2-yl)-2,5-diphenyltetrazolium bromide (MTT) was purchased from Biosharp Biotechnology Company (Beijing, China). 1,10-phenthroline and DMSO were purchased in the Guangzhou chemical reagent factory (Guangzhou). 4′,6-diamidino-2-phenylin-dole (DAPI) was obtained from Equation Biotechnology Co., Ltd. (Beijing, China). NMR spectra were performed with DMF-d_7 as solvent and tetramethylsilane (TMS) as an internal standard at AVANCE III 500 MHz nuclear magnetic resonance spectrometer (Bruker Bio-Spin, Switzerland) at room temperature. HRMS was detected through direct injection in the Xevo G2-XS QT mass analyzer (Waters, USA). UV–Visible and emission spectra were measured in the UV-2550 ultraviolet spectrophotometer and RF-5301PC fluorescence spectrophotometer (Shimadzu, Japan). The absorbance of microplates was recorded in a Multiskan™ FC Microplate Photometer (Thermo Fisher Scientific, USA). The apoptosis and cell cycle distribution were performed using FACS Calibur flow cytometer (BD, USA).

2.2. Synthesis of complexes

2.2.1. Synthesis of $[Ir(piq)_2(THPIP)]PF_6$ (*Ir1*)

A mixture of THPIP (0.212 g, 0.5 mmol) [20] and cis-$[Ir(piq)_2Cl]_2{\bullet}H_2O$ (0.338 g, 0.25 mmol) [21] was dissolved in 42 mL of dichloromethane and methanol (V:V = 2:1) and refluxed at 40 °C for 6 h under argon to produce a reddish-brown solution. After cooled to room temperature, an excess of ammonium hexafluorophosphate solution was added into the reddish-brown solution and stirred for 30 min. The obtained precipitate was washed thoroughly with dichloromethane. The crude product was purified by column chromatography. Neutral alumina (100–200 mesh, pH range 7 ± 0.5) was loaded on the column, and a mixture of dichloromethane and acetone (V:V = 3:1) was used as eluent. The pure **Ir1** product was obtained by evaporation under reduced pressure. Yield: 71.7%. Anal Calcd for $C_{57}H_{48}N_6OPF_6Ir$: C, 58.50, H, 4.13, N, 7.18%. Found: C, 58.31, H, 4.24, N, 7.36%. HRMS (CH_3CN): Calcd for $C_{57}H_{48}N_6OPF_6Ir$: m/z = 1025.3523 $[(M\text{-}PF_6)^+]$. Found: m/z = 1025.3558 $[(M\text{-}PF_6)^+]$ (**Fig. S1a,** supporting information). ^1H NMR (DMF-d_7, 500 MHz, **Fig. S1b,** supporting information): δ 9.14 (d, 4H, J = 8.5 Hz), 8.50 (d, 3H, J = 8.0 Hz), 8.07 (d, 2H, J = 8.0 Hz), 8.03 (s, 1H), 7.97–7.88 (m, 7H), 7.63 (d, 2H, J = 6.5 Hz), 7.54 (d, 2H, J = 6.5 Hz), 7.34 (s, 1H), 7.20 (t, 2H, J = 7.0 Hz), 6.98 (t, 2H, J = 7.5 Hz), 6.49 (d, 2H, J = 7.5 Hz), 1.54 (s, 9H), 1.39 (s, 9H). ^{13}C NMR (DMF-d_7, 125 MHz, **Fig. S1c,** supporting information): 173.49, 170.15, 156.65, 147.53, 144.74, 142.82, 138.64, 137.09, 133.78, 133.49, 132.34, 131.99, 130.77, 129.36, 128.27, 127.68, 127.38, 123.73, 123.69, 123.36, 33.00, 21.89.

2.2.2. Synthesis of $[Ir(bzq)_2(THPIP)]PF_6$ (*Ir2*)

The complex **Ir2** was synthesized in an identical method described for complex **Ir1**, with cis-$[Ir(bzq)_2Cl]_2{\cdot}H_2O$ [21] in place of cis-$[Ir(piq)_2Cl]_2{\cdot}H_2O$. The yellow product was obtained. Yield: 64.4%. Anal Calcd for $C_{53}H_{44}N_6OPF_6Ir$: C, 56.93, H, 3.97, N, 7.52%. Found: C, 56.80, H, 3.78, N, 7.77%. HRMS (CH_3CN): Calcd for $C_{53}H_{44}N_6OPF_6Ir$: m/z = 973.3210 $[(M\text{-}PF_6)^+]$ (**Fig. S2a,** supporting information). Found: m/z = 973.2503 $[(M\text{-}PF_6)^+]$. ^1H NMR (DMSO-d_6, 500 MHz, **Fig. S2b,** supporting information): δ 9.02 (d, 4H, J = 8.0 Hz), 8.41 (d, 2H, J = 8.0 Hz), 8.27 (s, 1H), 8.00 (d, 1H, J = 7.5 Hz), 7.90–7.85 (m, 5H), 7.46 (d, 2H, J = 6.5 Hz), 7.38 (d, 2H, J = 6.5 Hz), 7.23 (s, 1H), 7.17 (t, 2H, J = 7.5 Hz), 6.96 (t, 2H, J = 7.5 Hz), 6.33 (d, 2H, J = 7.0 Hz), 1.48 (s, 9H), 1.35 (s, 9H). ^{13}C NMR (DMSO-d_6, 125 MHz, **Fig. S2c,** supporting information): 174.08, 167.13, 158.53, 158.31, 156.63, 156.47, 152.73, 152.66, 151.10, 150.67, 149.58, 148.44, 142.41, 142.31, 139.69, 139.50, 135.76, 134.21, 131.74, 131.52, 130.54, 129.72, 128.71, 126.22, 124.76, 123.39, 123.02, 122.56, 122.29, 36.86, 23.06.

2.3. Cell culture

The cell lines used in this paper were all cultured in a medium containing 10% fetal bovine serum, HepG2, A549, HeLa and LO2 were cultured in DMEM high glucose medium, and BEL-7402 cells were cultured in RPMI-1640 medium. The cells used for drug administration and cell experiments were cultured in 6-well, 12-well, or 96-well cell culture plates.

2.4. Studies on cytotoxicity in vitro

The viability of cells treated by complexes **Ir1** and **Ir2** was evaluated by 3-(4,5-dimethylthiazol-2-yl)-2,5-diphenyltetrazolium bromide (MTT) method [22]. The cells were plated in 96-well microplates (1×10^4 cells per well) and cultured overnight in a 5% CO_2 incubator at 37 °C. Next day, when the cell density increased to about 50% ~ 60%, the cells were treated with different concentrations of the complexes (1.56, 3.125, 6.25, 12.5, 25, 50 and 100 μM) for 48 h (the complexes were dissolved in DMSO and the final concentration of DMSO is less than 0.05%). Then MTT (9:1, *v*/v) was added into every well and incubated at 37 °C for 4 h. The purple formazan product was dissolved with 100 μL dimethyl sulfoxide. Finally, a microplate reader was used to detect the absorbance value at a wavelength of 490 nm. The cell viability was calculated according to the following equation:

$$\text{Viability}\% = \left(\left(A_{\text{sample}} - A_{\text{medium control}}\right)/\left(A_{\text{cell control}} - A_{\text{medium control}}\right)\right) \times 100$$

Whereas A_{sample}, A_{medium} and A_{blank} are the absorbance values of sample, medium and control.

The IC_{50} values were obtained by plotting the percentage of cell viability versus concentration on a logarithmic graph and reading off the concentration at which 50% of cells remained viable relative to the control. Each experiment was repeated at least three times to obtain mean values.

2.5. Apoptosis assay by flow cytometry

Flow cytometry is an effective method to distinguish between non-apoptotic cells and apoptotic cells. BEL-7402 cells in a logarithmic growth phase were treated with IC_{50} concentration of the complexes for 48 h, the culture medium was discarded, the cells were collected by centrifugation and stained with Annexin V-FITC and incubated at 37 °C for 15 min, finally, the cells were detected using flow cytometry.

2.6. Western blot analysis

BEL-7402 cells were cultured in 6-well culture plates at a density of 4×10^5 cells/well. A blank control group was set, and BEL-7402 cells were treated with IC_{50} concentration of **Ir1** and **Ir2** for 24 h, then washed with ice-cold PBS, and lysed with the RIPA buffer on ice for 20 min. Next, the solution was centrifuged at 4 °C for 15 min. After centrifugation, the concentration of total protein was measured using the BCA protein assay kit. The electrophoresis process was performed on SDS-PAGE with equal

proteins. Then, the separated proteins were absorbed into PVDF membranes. Blocked for 70 min at room temperature and incubated with the primary antibody overnight at 4 °C. Incubated with dilutions of respective secondary antibodies coupled with horseradish peroxidase on ice for 70 min. Finally, the immune complexes were detected using the ECL method.

2.7. Glutathione (GSH) measurement

BEL-7402 cells (4×10^5 cells per well) were seeded in six-well plates overnight. After treatment with IC_{50} concentration of **Ir1** and **Ir2** for 24 h, the cells were trypsinized and washed twice with PBS. Glutathione assays were performed using the GSH Assay Kit (Beyotime Biotechnology, China) according to the manufacturer's protocol, the absorbance at 412 nm was measured, and then the GSH content was calculated.

2.8. Malondialdehyde (MDA) measurement

BEL-7402 cells treated with IC_{50} of **Ir1** and **Ir2** for 24 h were washed twice with PBS and then the cells were lysed with a mixture of RIPA (50 mM Tris (pH 7.4), 150 mM NaCl, 1% NP-40, 0.5% sodium deoxycholate) and PMSF (phenylmethanesulfonylfluoride). Then the cells were centrifuged at 12,000 ×*g* for 10 min at 4 °C to remove insoluble cell debris. Total protein was determined using the Pierce BCA Protein Assay Kit (Beyotime Biotechnology, China). To detect lipid peroxidation, the lysates obtained from the above operations were assayed by the MDA Assay Kit (Beyotime Biotechnology, China). Through calculating the protein content and the MDA content in the solution, the amount of MDA in the original sample can be obtained.

2.9. Immunofluorescence analysis

BEL-7402 cells (4×10^5 cells/well) were seeded in 12-plate overnight, the cells were treated with IC_{50} concentration of **Ir1** and **Ir2** for 24 h, the cells were fixed in 75% ethanol for 30 min. Then the cells were blocked with an immunostaining blocking solution at 4 °C for 1 h. Subsequently, the cells were washed three times with immunostaining solution and incubated with CRT antibody, HMGB1 antibody, and HSP70 antibody for 12 h. After washing with immunostaining solution and incubation with secondary antibody for 1 h in the dark, then the cells were stained with Hoechst for 30 min, washed with cold PBS, and immediately photographed under Image Xpress Micro XLS.

2.10. RNA sequence analysis

BEL-7402 cells were inoculated in 6-well culture plates (5×10^5 cells) and incubated in a 37 °C incubator for 24 h. The BEL-7402 cells were exposed to $2 \times IC_{50}$ concentration of **Ir1** for 24 h. Adherent cells were washed twice using pre-chilled PBS. The appropriate amount of RNA extraction solution (Servicebio, China) was added, and cells were well blown using a pipette to lyse them adequately, followed by isolation of total RNA using Trizol Reagent (Invitrogen Life Technologies), after which the concentration, quality and integrity were determined using a NanoDrop spectrophotometer (Thermo Scientific). Sequencing libraries were generated using the TruSeq RNA Sample Preparation Kit (Illumina, San Diego, CA, USA). To select cDNA fragments with a length of preferably 200 bp, library fragments were purified using the AMpure XP system (Beckman Coulter, Beverly, CA, USA). The library fragments were then quantified using Agilent high-sensitivity DNA analysis on a BioAnalyst 2100 system (Agilent, Santa Clara, CA, USA). Finally, the sequencing library was sequenced on a Hiseq platform (Illumina) by Shanghai Personal Biotechnology Cp. Ltd. (China).

The experimental procedures for luminescence quantum yields, cell uptake analysis, wound scratch, colony formation, Cell cycle distribution, location assays of **Ir1** and **Ir2** at the mitochondria, the change of mitochondrial membrane potential, intracellular Ca^{2+} levels, intracellular ROS content, autophagy and molecular mocking studies can be found in the supporting information.

2.11. Data analysis

All data were expressed as mean ± SD. Statistical significance was evaluated using *t*-tests. Differences were considered significant when the $^*P$ value was less than 0.05.

3. Results and discussion

3.1. Synthesis and characterization

The synthetic route for ligand and its two iridium(III) complexes is shown in Scheme 1. The ligand THPIP was prepared according to the previously reported methods [20]. The complexes $[Ir(piq)_2(THPIP)]PF_6$ (**Ir1**) and $[Ir(bzq)_2(THPIP)]PF_6$ (**Ir2**) were synthesized by the direct reaction with THPIP and precursors in dichloromethane and methanol. The complexes were characterized by elemental analysis, HRMS, ^1H NMR, and ^{13}C NMR. In the HRMS spectra, the determined molecular weights are consistent with the expected values. In the ^1H NMR spectra, the peaks of 8.03 (s, 1H) and 7.34 (s, 1H) for **Ir1**, 8.27 (s, 1H) and 7.23 (s, 1H) for **Ir2** are attributed to the hydrogen atoms at the position of b and a, respectively. However, the peak for the proton on nitrogen atom of the imidazole ring was not observed, which may be caused by metal coordination inducing electron deficiency in the ligand, therefore, the NH proton of the imidazole ring is very active and easy to be exchanged between the two imidazole nitrogen atoms in solution. In addition, the peaks for the proton in the phenol hydroxyl (-OH) are not observed. Similar results can be found in the literature [23]. In the ^{13}C NMR spectra, the peaks of 33.00 ppm for **Ir1**, 36.86 ppm for **Ir2** are assigned the tert-butyl carbon atoms ($-C(CH_3)_3$), while the peaks of 21.89 ppm for **Ir1** and 23.06 ppm for **Ir2** are attributed to the methyl carbon atoms ($-CH_3$).

The stability of the complexes **Ir1** (30 μM) and **Ir2** (9.8 μM) in PBS solution was investigated by UV–Vis spectra, as shown in **Fig. S3a** and **3b** (supporting information), no change in the peak shape at 0 and 24 h was found, indicating that the complexes are stable. Owing to low solubility, some precipitates were observed at 24 h, therefore, the absorbance decreases. In addition, we also determined the UV–Vis spectra of ligand, $[Ir(piq)_2Cl]\cdot H_2O$ and $[Ir(bzq)_2Cl]\cdot H_2O$ (**Fig. S3c**, supporting information), the peak shapes are different with the complexes **Ir1** and **Ir2**, which further suggests that the complexes are stable. The luminescence of complexes **Ir1** (30 μM, $\lambda_{ex} = 357$ nm) and **Ir2** (9.8 μM, $\lambda_{ex} = 354$ nm) in PBS solution are obtained at room temperature, the maximum for **Ir1** and **Ir2** appears at 611 nm (**Fig. S3d,** supporting information). The luminescence quantum yield (Φ) of the complexes was determined according to the literature [24], $[Ru(bpy)_3]^{2+}$ ($\Phi = 0.04$, methanol) was used as a reference. The luminescence quantum yields for **Ir1** and **Ir2** were determined to be 0.30, and 0.04, respectively. The time-resolved fluorescence decay profiles for complexes were determined using time-correlated single-photon counting (TCSPC) spectroscopy. The average fluorescence lifetimes of complexes **Ir1** and **Ir2** are 189.5 and 16.1 ns, respectively.

The purity of the complexes was determined by HPLC using methanol and water ($V_{methanol}$:$V_{H2O} = 60{:}40$ for **Ir1**, 80:20 for **Ir2**) as mobile phase, during a period of 30 min, only a peak was observed, indicating that the complexes are pure (**Fig. S3e**) (supporting information), the values of the purity for **Ir1** and **Ir2** are 97.41 and 97.00%, respectively.

3.2. Cellular uptake studies

It is very important to study whether the complexes can effectively enter the cells. Researchers have proposed several pathways for the complexes to enter the cells including passive diffusion through the

Table 1
IC_{50} (μM) values of **Ir1, Ir2, THPIP** and cisplatin toward the selected cancer and normal cells for 48 h.

Complex	BEL-7402	A549	HepG2	HeLa	LO2
THPIP	37.4 ± 1.4	38.1 ± 1.4	>100	27.2 ± 1.0	45.4 ± 2.3
Ir1	29.9 ± 4.6	>100	>100	>100	>100
Ir2	9.8 ± 1.8	>100	>100	25.7 ± 0.8	>100
Cisplatin	15.4 ± 4.1	6.5 ± 0.5	9.1 ± 0.9	5.7 ± 1.7	18.5 ± 0.7

Data for cisplatin from Ref [27].

membrane, transport proteins, and endocytosis [25]. To confirm whether the complexes can enter the cells, the cellular uptake was investigated under Image Xpress Micro XLS. After the treatment of BEL-7402 cells with IC_{50} concentration of **Ir1** and **Ir2** for 24 h, as shown in **Fig. S4a** (supporting information), the complexes emit weak green fluorescence, the cell nuclei were stained blue with DAPI, the overlap of green and blue fluorescence indicated that the complexes may enter the cell and distribute in the cytoplasm. We also quantitatively determined the cell uptake using flow cytometry, as shown in **Fig. S4b** (supporting information), BEL-7402 cells were treated with IC_{50} concentration of **Ir1** or **Ir2** for 24 h, the green fluorescence intensity increased by 3.08 and 4.70 times for **Ir1** and **Ir2** compared with that in the control, while the treatment of A549 cells with IC_{50} concentration of **Ir1** and **Ir2** for 24 h, the green fluorescence intensity only increased by 1.27 and 1.16 times, respectively. Hence, the cellular uptaken amounts of the complexes by BEL-7402 cells are more than those by A549 cells.

3.3. Cytotoxic activity assay of the complexes toward cancer cells

3-(4,5-dimethylthiazol-2-yl)-2,5-diphenyltetrazolium bromide (MTT) method was used to evaluate the cytotoxic activity of the complexes **Ir1**, and **Ir2** against cancer cells BEL-7402, HepG2, A549, HeLa, and liver cell line (LO2), the culture medium was used as a blank control. As depicted in Table 1, complex **Ir1** only shows moderate cytotoxic activity against BEL-7402 cells, no cytotoxicity toward HepG2, HeLa and A549 cells. While complex **Ir2** exhibits high cytotoxic activity against BEL-7402, no cytotoxic activity toward HepG2 and A549 cells, which is related to the uptaken amount of the complexes by different cancer cells. Interestingly, the complexes reveal no cytotoxic efficacy toward normal liver LO2 cells. Comparing the IC_{50} value, **Ir2** shows higher cytotoxic effect on BEL-7402 cells than that of cisplatin, but lower than those of iridium(III) complexes $[Ir(bzq)_2(FTTP)](PF_6)$ (FTTP = 2-(3-fluoronaphthalen-2-yloxy)-1,4,8,9-tetraazatriphenylene, IC_{50} = 1.6 ± 0.09 μM) and $[Ir(piq)_2(FTTP)](PF_6)$ (IC_{50} = 1.1 ± 0.02 μM) [26]. In our previous work [20], we synthesized three Ru(II) complexes Ru1, Ru2 and Ru3 containing THPIP ligand (Scheme 1), the anticancer activity of the Ru(II) complexes against BEL-7402 cells is lower than that of Ir(III) complex **Ir2**, but their cytotoxicity is higher than **Ir1** against BEL-7402 cells, moreover, the anticancer efficacy of complexes Ru1 (IC_{50} = 8.6 ± 1.1 μM), Ru2 (IC_{50} = 13.1 ± 1.1 μM) and Ru3 (IC_{50} = 7.3 ± 1.4 μM) is higher than Ir(III) complexes toward A549 cells. Although Ru(II) and Ir(III) complexes containing the same main ligand THPIP, different metal ion and different ancillary ligand result in different anticancer effect on the same cancer cells. Additionally, we also determined the IC_{50} values of the complexes against A549 and HepG2 cells upon irradiation (65 w LED lamp, white light, λ = 450–465 nm, 5.2 J cm^{-2}). After the addition

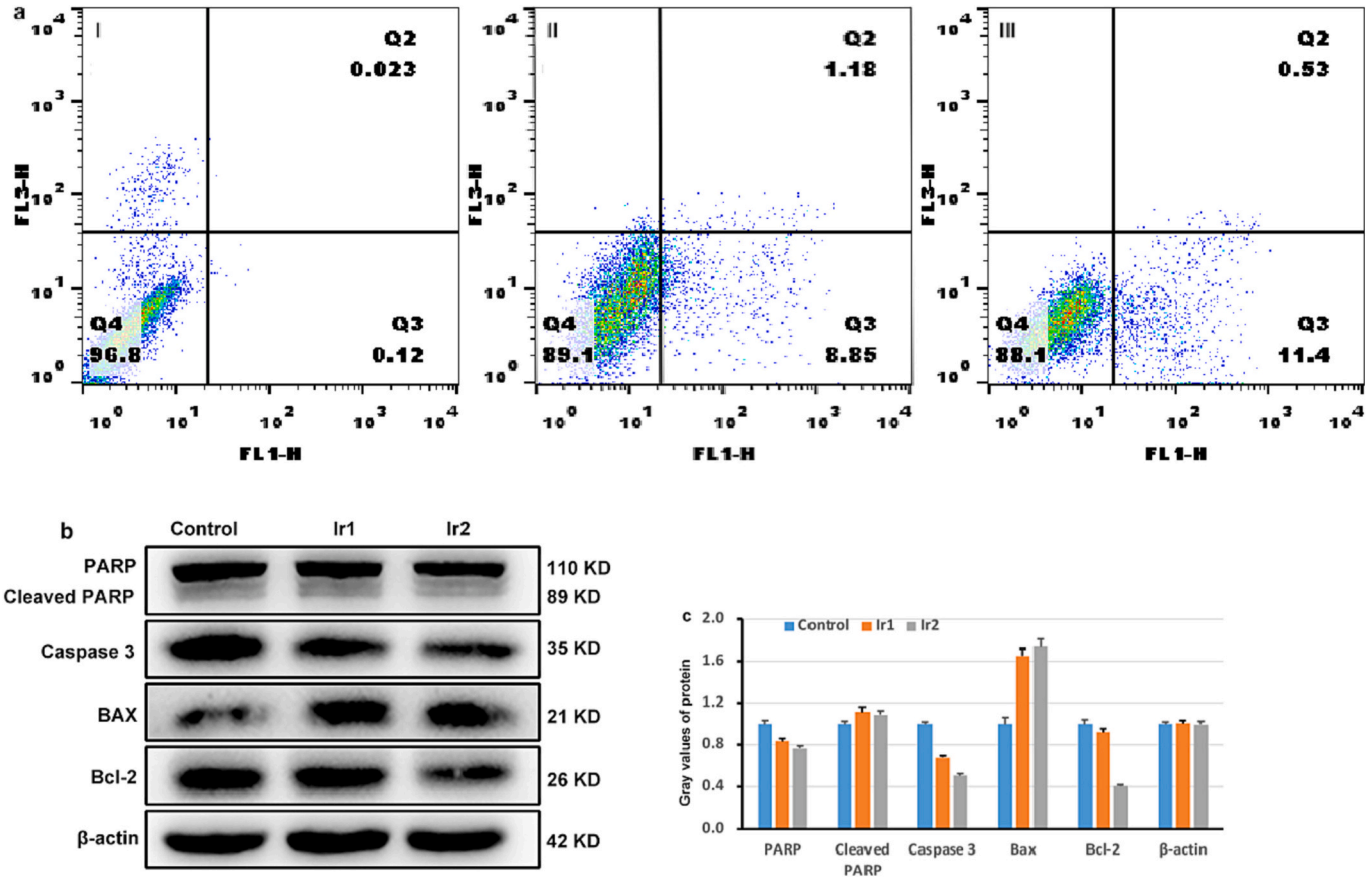

Fig. 1. (a) The apoptosis was performed after BEL-7402 cells (I) were incubated with IC_{50} concentration of **Ir1** (II), and **Ir2** (III) for 48 h by flow cytometry. (b) The expression of caspase 3 and Bcl-2 family proteins in BEL-7402 cells treated with IC_{50} concentration of the complexes for 24 h, β-actin was used as an internal control. (c) The gray values of PARP, Cleaved PARP, Caspase 3, Bax and Bcl-2 proteins.

of the complexes, 30 min of irradiation to the cells and continued to incubate for 48 h, the IC_{50} values of the complexes **Ir1** and **Ir2** toward A549 and HepG2 cells are more than 100 μM, which indicates that irradiation has no influence on the cytotoxic activity. To further investigate the antiproliferative mechanism of **Ir1** and **Ir2**, BEL-7402 cells were chosen for the following cell experiments.

3.4. *Effects of **Ir1** and **Ir2** on the inhibition of migration and colony-forming assay*

Cell migration is the most frequently used in vitro biological method to test the drug efficacy. As depicted in **Fig. S5a** and **b** (supporting information), the wound width of the blank group was significantly reduced. After the cells were treated with IC_{50} concentration of the complexes **Ir1** and **Ir2** for 24 h, the distance between the wound edges increased compared with the control group, which indicated that complexes effectively inhibit the migration of BEL-7402 cells. The colony formation is used to test the proliferative capacity of cancer cells [28]. As demonstrated in **Fig. S5c** and **d** (supporting information), the number of cells was significantly reduced compared to the control group after an exposure of BEL-7402 cells to IC_{50} concentration of the complexes for 24 h. Focal adhesion kinase (FAK) is overexpressed in some human tumors such as liver and breast cancers and it can play an important role in tumor progression [29,30]. Reduced FAK expression was associated with loss of adhesion, reduced migration, and induction of apoptosis [31]. As shown in **Fig. S5e** and **f** (supporting information), the complexes downregulated the expression of FAK protein compared with that in the control group. All the above results demonstrated that **Ir1** and **Ir2** significantly inhibit the migration of BEL-7402 cells.

3.5. *Effects of **Ir1** and **Ir2** on cell cycle arrest*

Loss of cell cycle control is a hallmark of tumorigenesis [32]. The effect of complexes on cell cycle progression was investigated using flow cytometry. As given in **Fig. S6a** (supporting information), the treatment of BEL-7402 cells (I) with IC_{50} concentration of **Ir1** (II) and **Ir2** (III) increased the S-phase portion in the cells and resulted in a corresponding decrease in G0/G1 portion compared with that in the control group. At the same time, there was only a slight decrease in the G2/M phase. The results showed that the complexes induce cell cycle arrest at the S phase. Protein p21, a founding member of the cell cycle protein-dependent kinase inhibitors, is an important cell cycle regulator that inhibits a variety of cell cycle proteins, and it is also an essential target gene to cause cell cycle arrest [33]. As shown in **Fig. S6b** and **c** (supporting information), the complexes upregulated the expression of p21 protein compared with that in the control. The results suggested that **Ir1** and **Ir2** induce cell cycle arrest in the S phase and increase the expression of p21 protein.

3.6. *Apoptosis detection*

Apoptosis is a critical mechanism for maintaining intracellular life-death balance to prevent cancer and other related diseases [34]. The features of apoptotic cell mainly include condensation of chromatin material, fragmentation of nuclear DNA, cell shrinkage, dynamic membrane blebbing, and loss of adhesion. To further study the ability of the complexes causing cell death, the effect of complexes on apoptosis in BEL-7402 cells was determined using the Annexin V-FITC/propidium iodide (PI) method. The results are shown in Fig. 1a, the early apoptotic rate in the control group (I) was 0.12%. When BEL-7402 cells were treated with IC_{50} concentration of complexes **Ir1** or **Ir2** for 48 h, the percentage of early apoptosis was 8.85% for **Ir1** (II) and 11.4% for complex **Ir2** (III). The results indicated that the complexes can effectively induce early apoptosis of BEL-7402 cells.

It is well known that apoptosis is mainly achieved through exogenous death receptor- pathway and/or endogenous mitochondria pathway. The mitochondrial pathway is precisely regulated by signaling of multiple physiological activities, and Bcl-2 family proteins and caspase cascade reaction [35,36]. Therefore, the changes in the expression levels of the corresponding proteins can directly reflect the extent of apoptosis [37]. The results were presented in **Fig. 1b** and **c**, the expression of apoptosis-related proteins caspase 3 and Bcl-2 was significantly decreased in the **Ir1-** and **Ir2**-treated groups compared with that in the control group. Under normal conditions, caspase 3 exists in the form of the zymogen, and once the cells are stimulated to produce apoptotic signals, it is shear-activated by caspase 8/9/10 to play a pro-apoptotic role [38]. The reduction of the expression of caspase 3 indicated that it was sheared intracellularly, which implied the smooth transmission of apoptotic signals. BAX is a core member of the Bcl-2 family of proteins, which regulates the balance between cell survival and death [39]. The expression of the anti-apoptotic protein BAX was increased compared to the blank group. PARP is the main substrate for activation of caspase-3 and cleaved PARP is an apoptosis-specific biomarker [40]. Thus, inhibition of PARP expression can block the DNA repair process and accelerate apoptosis. Western blotting assay showed that the expression level of PARP was decreased, which further confirmed that **Ir1** and **Ir2** can activate the pro-apoptotic protein BAX through targeting Bcl-2 family proteins and cascade enzyme proteins, while inhibiting the activation level of Bcl-2, promoting caspase 3 shearing to deliver and amplify apoptotic signals and eventually inhibiting the repair of damaged DNA to lead to apoptosis of BEL-7402 cells.

3.7. *Complex-mitochondrial co-localization and membrane potential detection*

Due to the intrinsic fluorescent properties of iridium(III) complexes, their subcellular localization can be readily analyzed using confocal microscopy [41]. DAPI nuclear staining and mitochondrial staining were used to identify subcellular compartments where **Ir1** and **Ir2** accumulated. As seen **Fig. S7a** (supporting information), the cell nuclei were stained blue with DAPI, the mitochondria were stained red with Mito Tracker Red, and the complexes emit weak green fluorescence, the overlap of red and green fluorescence indicated that **Ir1** and **Ir2** were predominantly accumulated in the mitochondria. Pearson's colocalization coefficients (PCC) were calculated by analyzing the red and green fluorescence intensity (Image pro plus 6.0 software) in 50 cells according to literature [42]. The PCC values for **Ir1**, **Ir2** are 0.93 and 0.97, which demonstrated an existence of positive correlation. Mitochondrial ion channels, as emerging tumor targets as the regulation of these ion transport proteins, may affect mitochondrial membrane potential (MMP) and it is an early apoptotic marker [14,43,44]. The reduction of MMP is a key factor in the process of apoptosis [45].

To determine whether Ir(III) complex-induced apoptosis occurred accompanied by the mitochondrial damage, we determined the changes of MMP in BEL-7402 cells with 5,5′-6,6′-tetrachloro-1,1′-3,3′-tetrethylbenzimidalylcarbocyanine iodide (JC-1) as fluorescence probe. JC-1 emits red fluorescence as an aggregate at high MMP, and JC-1 emits green fluorescence as a monomer corresponding to low MMP [46–48]. As shown **Fig. S7b** (supporting information), after BEL-7402 cells were treated with CCCP, IC_{50} concentration of the complexes **Ir1** and **Ir2** for 24 h, there was a significant decrease in red fluorescence and an increase in green fluorescence compared with that in the control group. The ratio of red/green fluorescence intensity is shown in **Fig. S7c** (supporting information), the red/green ratio in the CCCP, **Ir1** and **Ir2**-treated groups reduced compared with that in the control group, further indicating a decrease of red and an increase of green fluorescence intensity. These results indicated that the complexes co-localize in the mitochondria, induce a decrease in the mitochondrial membrane potential and finally cause mitochondrial damage.

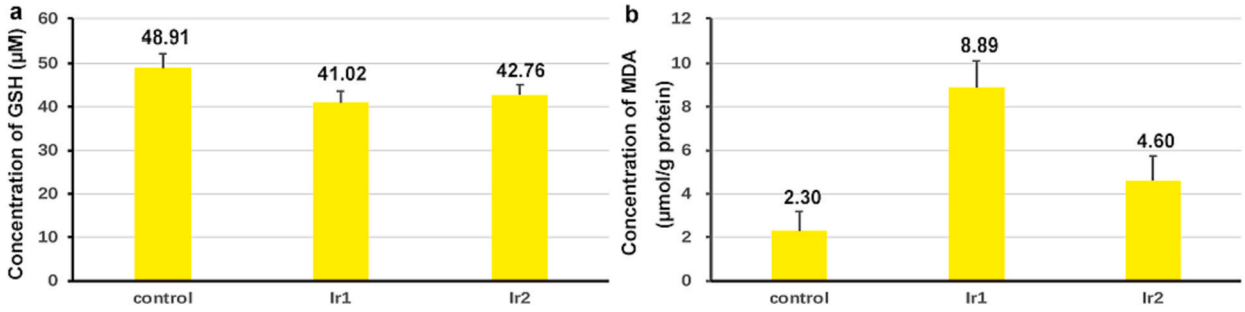

Fig. 2. Measurements of GSH levels (a) and MDA content (b) after BEL-7402 cells were treated with IC_{50} concentration of **Ir1** and **Ir2** for 24 h.

3.8. Analysis of intracellular Ca^{2+} levels

Ca^{2+} release from the mitochondria play a key role in cell physiology [49]. To determine the change of intracellular Ca^{2+} concentration, Fluo-3 AM was used as a fluorescent probe. As shown in **Fig. S8a** (supporting information), the green fluorescence in the control group was extremely weak, indicating a low Ca^{2+} level in the BEL-7402 cells. After the cells were treated with IC_{50} concentration of the complexes for 24 h, the green fluorescence significantly increased, indicating an increase of intracellular Ca^{2+} content. To exclude the cross-interference of the weak green fluorescence caused by the complexes, the green fluorescence intensity was determined according to the following equation:

Igreen fluorescence = Igreen fluorescence of the complexes in the cells + Fluo − 3 AM–Igreen fluorescence of the complexes in the cells

As shown in **Fig. S8b** (supporting information), the green fluorescence intensity increased by 1.88 times for **Ir1** and 1.67 times for **Ir2** compared with that in the control group after BEL-7402 cells were treated with IC_{50} concentration of **Ir1** and **Ir2** for 24 h, which further confirms that the complexes can enhance intracellular Ca^{2+} concentration.

3.9. Qualitative and quantitative measurement of ROS generation

Mitochondrial dysfunction can lead to ROS production and enhance cell mobility by elevating cell membrane Ca^{2+} levels. The 2′,7′-Dichlorodihydrofluorescein diacetate (DCFH-DA) probe is the most common and sensitive tool for the detection of intracellular ROS levels [50]. To determine whether complex-induced apoptosis in BEL-7402 cells was associated with ROS production, we examined the level of intracellular ROS. As shown in **Fig. S9a** (supporting information), only faint green fluorescence was found in the control group, while BEL-7402 was treated with IC_{50} concentration of complexes **Ir1** and **Ir2** for 24 h, a bright green fluorescence was observed. The increased green fluorescence intensity indicated that the complexes increased intracellular ROS content. To exclude the cross-interference of green fluorescence emitted by the complexes, the green fluorescence intensity was calculated according to the following equation:

Igreen fluorescence = Igreen fluorescence of the complexes in the cells + DCHF − DA–Igreen fluorescence of the complexes in the cells

The quantified green fluorescence intensity of DCF is shown in **Fig. S9b** (supporting information), the green fluorescence intensity was significantly increased by 1.89, 2.75 and 2.45 times for Rosup (positive control), **Ir1** and **Ir2** compared with that in the control. These results further show that the complexes are capable to increase intracellular ROS levels.

3.10. Determination of the intracellular glutathione (GSH) and malondialdehyde (MDA) levels

Glutathione (GSH) depletion is an early observed marker of apoptosis and participates in the detoxification and deactivation of metal-based anticancer complexes [51–53]. To further explore the effects of Ir(III) complex-induced ROS activation on mitochondria and apoptosis, the changes of intracellular GSH levels were determined. As shown in Fig. 2a, comparing to the control group, the intracellular GSH levels decreased by 16.13% and 12.57% after BEL-7402 cells were treated with IC_{50} concentration of complexes **Ir1** and **Ir2** for 24 h, respectively. Additionally, we also determined the ratio of GSH/GSSG (glutathione disulfide), in the control, the ratio of GSH/GSSG is 7.34 ± 1.87, after an exposure of BEL-7402 cells to IC_{50} concentration of **Ir1** or **Ir2** for 24 h, the ratios of GSH/GSSG are 3.73 ± 0.86 and 4.31 ± 0.25, respectively. Therefore, the complexes can reduce the content of intracellular GSH and cause an increase of oxidant stress.

Lipid oxidation or lipid peroxidation is one of the most common oxidative stress indicators, and it is also considered to be one of the pathological factors leading to chronic diseases. The most studied marker of lipid peroxidation is malondialdehyde (MDA), which directly represents oxidative damage to cells [54,55]. It is known that the treatment of cancer patients depletes the antioxidant SOD levels in biological systems, leading to increased lipid peroxidation, which is reflected in the increase of intracellular MDA levels [56]. As shown in Fig. 2b, compared to the control group, oxidized lipid products MDA levels increased 3.86-fold for complex **Ir1** and 2.00-fold for complex **Ir2**. Together, the above experimental results indicated that **Ir1** and **Ir2** can inhibit the production of GSH and increase the content of lipid peroxides MDA.

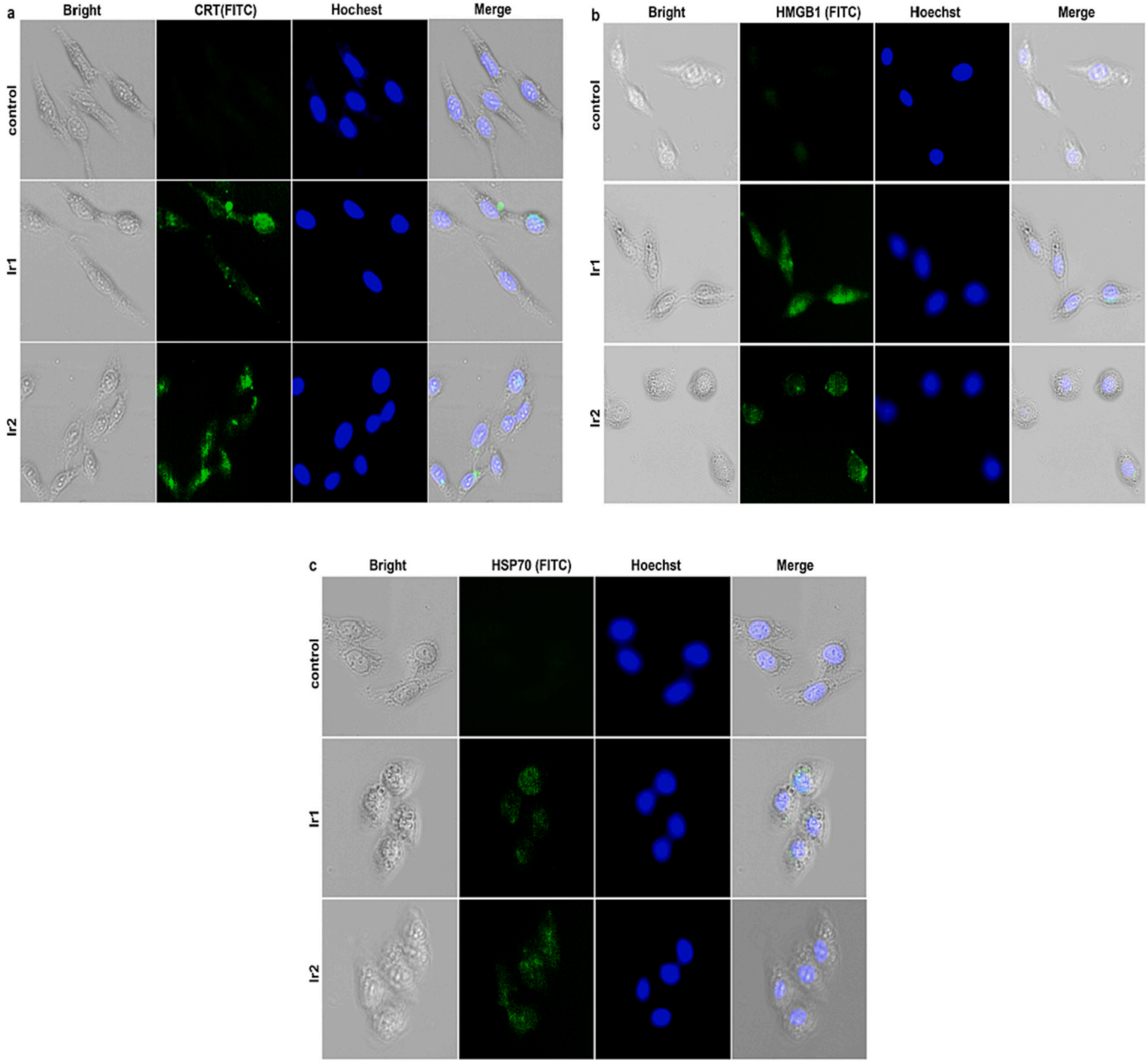

Fig. 3. CRT (a), HMGB 1 (b) and HSP 70 (c) were measured after the treatment of BEL-7402 with IC_{50} concentration of **Ir1** and **Ir2** for 24 h.

*3.11. **Ir1** and **Ir2** induced autophagy in BEL-7402 cells*

Autophagy plays a crucial regulatory role in drug-induced apoptosis, and dysregulation in autophagy may be one of the major factors contributing to sustained cell proliferation and development of tumors [57,58]. Anticancer agents have been shown to induce apoptosis and autophagy in cancer cells through the production of ROS [59]. To explore the effects of the complexes on autophagy, BEL-7402 cells were treated with IC_{50} concentration of the complexes for 24 h, the cells were stained with monodansylcadaverine (MDC), as shown in **Fig. S10a** (supporting information), the increased green fluorescence was discovered compared with that in the control, indicating that the complexes can induce autophagy.

One of the most common analytic methods for evaluating autophagy behavior is to quantify the microtubule-related protein MAP1LC3 (LC3) level by immunoblot [60]. LC3 is a marker of autophagosomes, which can be transferred from LC3-I to LC3-II when autophagy occurs [61,62]. Beclin-1 contains a BH3 structural domain that binds to B-cell lymphoma-2 (Bcl-2) protein, and the release of Beclin-1 from these proteins can induce autophagy [63]. As represented in **Fig. S10b** and **c** (supporting information), after treatment of BEL-7402 cells with IC_{50} concentration of **Ir1** and **Ir2** for 24 h, the expression levels of LC3-II and Beclin-1 proteins were increased, but the expression of p62 protein was decreased compared to the control group. These experimental results suggested that the complexes can effectively induce autophagy.

3.12. Determination of CRT, HSP70 and HMGB1

Immunogenic cell death (ICD) is a model for drug-induced tumor cell death that relies on the production of immune signals, induced by various stimuli including damage-associated molecular patterns (DAMPs) such as calmodulin (CRT), high mobility group box 1 (HMGB1) and heat shock protein (HSP)70 [64–66]. To evaluate the efficacy of the complexes on ICD, fluoresceine isothiocyanate (FITC) was used as

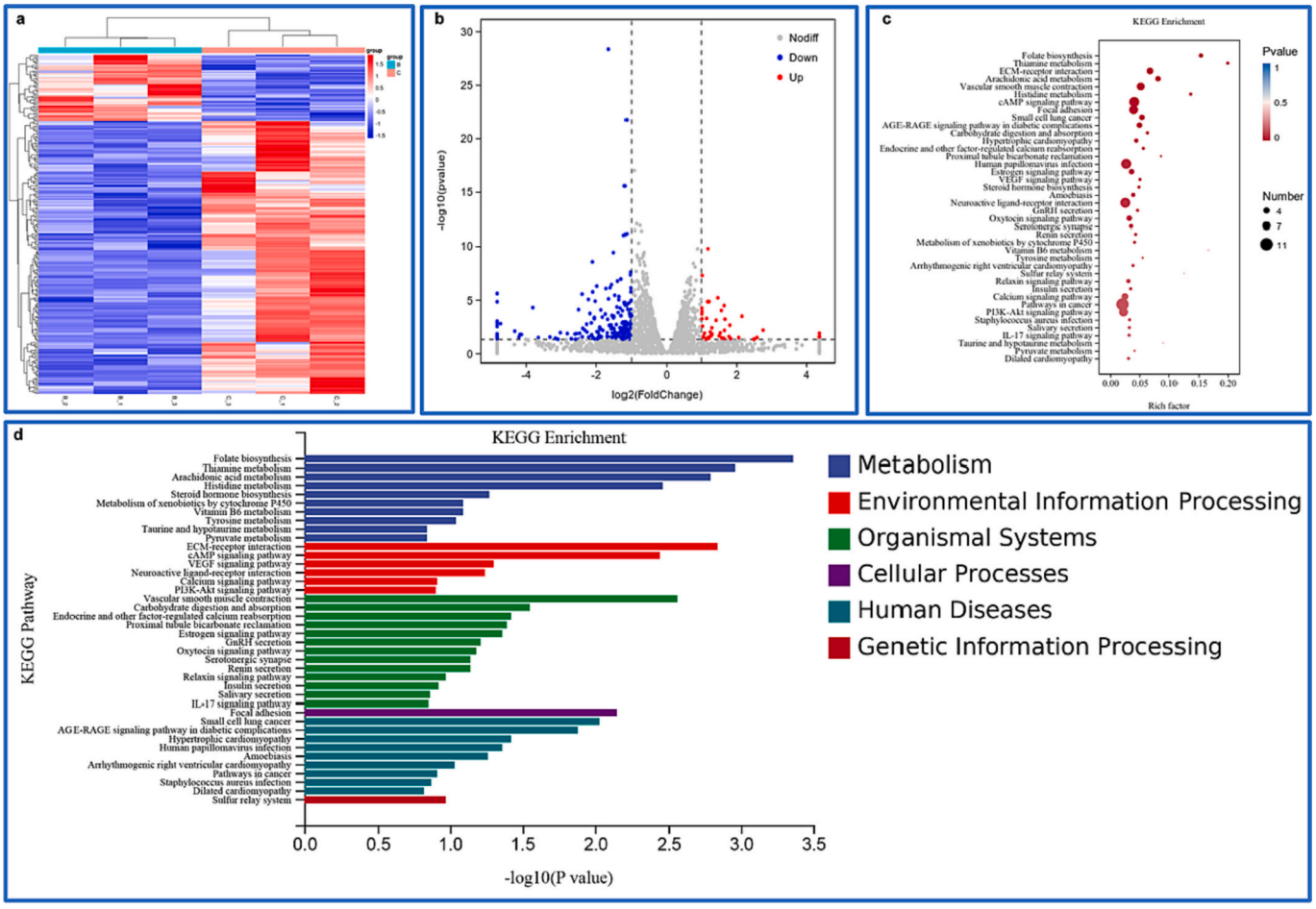

Fig. 4. Bioinformatics identified key pathways and biological processes associated with **Ir2** sensitivity in BEL-7402 cells. (a) Heat map, (b) Volcano map, (c and d) Kyoto encyclopedia of genes and genomes pathway analyses.

fluorescence probe. As shown in Fig. 3a, the fluorescence of intracellular CRT increased after the treatment of BEL-7402 cells with IC_{50} concentration of complexes **Ir1** and **Ir2** for 24 h compared that in the control. Thorburn et al. reported that autophagy can control the characteristics of dead cells by regulating the selective release of HMGB1 [67]. An important feature of ICD is the release of HMGB1 from the nucleus into the periphery of dead cells [68]. Next, we investigated whether HMGB1 can be released from the cells. As shown in Fig. 3b, a significant increase in the green fluorescence of HMGB1 was observed in the **Ir1** and **Ir2**-treated groups compared with that in the control. In addition, HSP70 accumulated significantly on the cell membrane after the treatment of the cells with **Ir1** and **Ir2** for 24 h (Fig. 3c) was also discovered. Taken

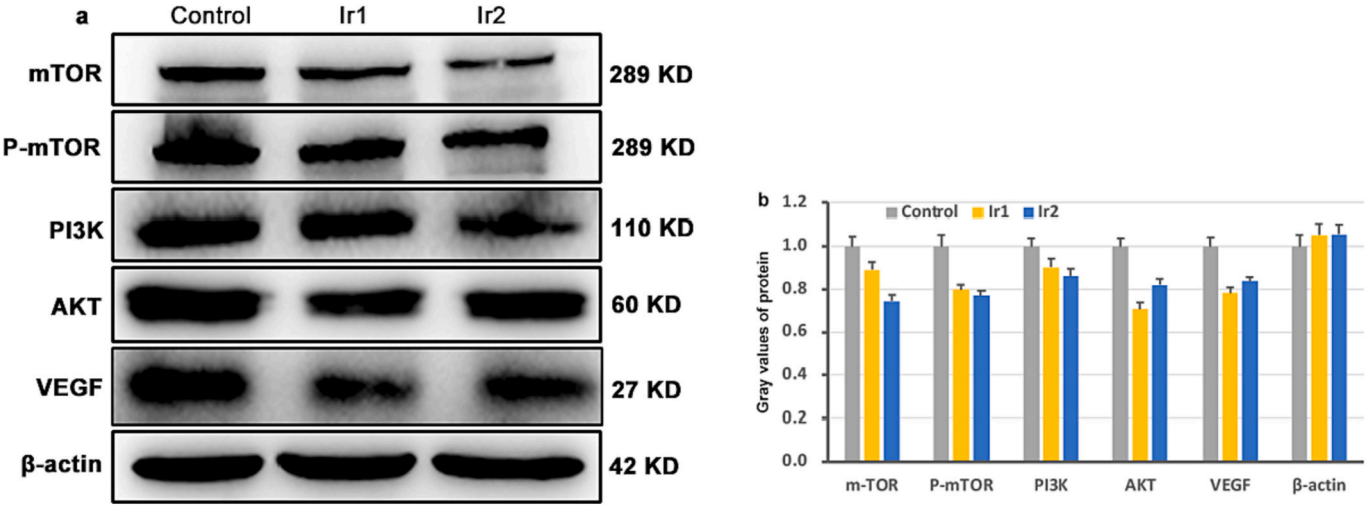

Fig. 5. (a) The expression of PI3K, AKT, mTOR, and p-mTOR was detected after BEL-7402 cells were treated with IC_{50} concentration of **Ir1** and **Ir2** for 24 h. (b) Gray values of proteins.

Table 2
Docking information for the 10 proteins with the corresponding **Ir1** and **Ir2**. The values are the lowest binding energies (kcal/mol) between the protins and **Ir1** and **Ir2.**

Complex	FAK	p21	PARP	Caspase 3	Bax	Bcl-2	p62	Beclin-1	mTOR	PI3K
Ir1	−8.4	−8.8	−6.7	−8.9	−5.3	−2.9	−4.5	−10.9	−9.4	−7.1
Ir2	−9.3	−9.5	−8.7	−7.7	−4.5	−5.6	−4.6	−9.4	−9.6	−6.6

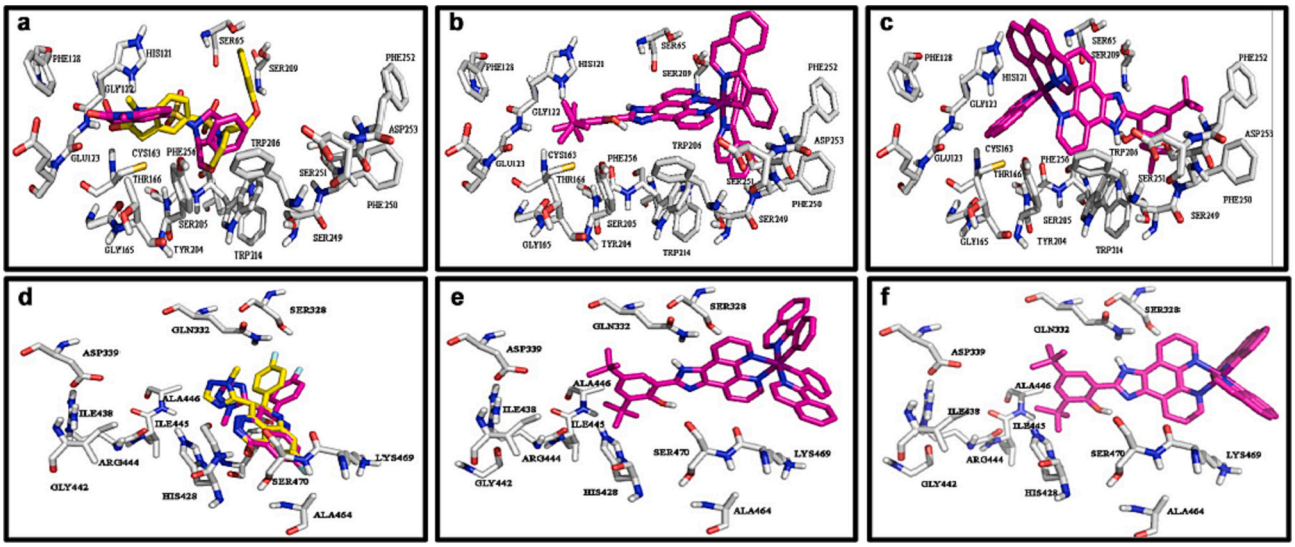

Fig. 6. Molecular docking of the complexes in caspase 3 (PDB: 1GFW) (a, method validation; b, **Ir1**; c, **Ir2**), PARP (PDB: 4PJV) (d, method validation; e, **Ir1**; f, **Ir2**).

together, these results suggested that the complexes can induce immunogenic cell death.

3.13. RNA sequencing assay

RNA sequencing (RNAseq) can detect different types of cancer and rare diseases and provides researchers insight into developing more effective therapies [69]. Shen et al. investigated RNA-seq data of autophagy-associated genes and found that enriched words from GO and KEGG enrichment analysis were associated with autophagy and multiple cancers including hepatocellular carcinoma [70]. To investigate in depth the role of **Ir2** in hepatocellular carcinoma tumorigenesis, we performed RNA-seq analysis of total RNA after a 24 h treatment of BEL-7402 cells with 2 × IC_{50} concentration of **Ir2** (Fig. 4a-d). Compared with the control group, 47 genes were up-regulated and 193 genes were down-regulated after **Ir2** treatment (**Fig. 4a** and **b**). After performing differential gene expression analysis and downstream gene set enrichment analysis, we found that the complex **Ir2** was mainly associated with Ca^{2+} ion signaling pathway, PI3K/AKT signaling pathway, VEGF signaling pathway and Focal adhesion (**Fig. 4c** and **d**). This was consistent with our previous study. The complexes inhibit cell migration and further induce apoptosis through Ca^{2+} ion signaling pathway, reducing FAK expression and activating the Focal adhesion signaling pathway. We also observed that the complexes can activate PI3K, AKT, and VEGF signaling pathways, which further demonstrates that the complexes induce apoptosis in BEL-7402 cells through inhibition of PI3K/AKT/mTOR signaling pathway.

3.14. Effect of *Ir1* and *Ir2* on the regulation of the PI3K/AKT/mTOR pathway

The results from RNA-sequence analysis indicates that the complexes induce apoptosis through inhibition of PI3K/AKT/mTOR signaling pathway. The PI3K (phosphatidylinositol 3-kinase)/AKT (protein kinase B)/mammalian target of rapamycin (mTOR) signaling pathway is involved in tumorigenesis and development. The mTOR signaling pathway is involved in cell metabolism and proliferation, which is key hallmarks of cancer [71]. The VEGF/PI3K/AKT signaling pathway is involved in cell proliferation, differentiation, apoptosis and vascular growth processes [72]. Inhibition of VEGF can reduce tumor angiogenesis and growth by inactivating the PI3K/AKT signaling pathway [73]. Western blotting assay was used to detect the expression of PI3K, AKT, mTOR, etc. As shown in Fig. 5**a** and **b**, after a 24 h treatment of BEL-7402 cells with IC_{50} concentration of the complexes, **Ir1** and **Ir2** reduced the phosphorylation level (P-mTOR), down-regulated the expression of PI3K, AKT, and mTOR compared with those in the control. The results provided evidence that the complexes induce apoptosis in BEL-7402 cell through inhibition of PI3K/AKT/mTOR signaling pathway. Hence, RNA-sequence analysis provides useful help for investigating the apoptotic mechanism.

3.15. Molecular docking studies

To confirm the above findings, we performed a molecular docking analysis of the compound structures to predict whether **Ir1** and **Ir2** interacted with the proteins including Bcl-2, PI3K, BAX, Caspase 3, PARP, FAK, mTOR, p62, p21 and Beclin-1 (these proteins were investigated in the autophagy, PI3K/AKT/mTOR signaling pathway, cell cycle arrest and invasion-related protein FAK). We first identify the space place of the complexes in the above proteins according to the method validation using crystallized and docking ligand, then we calculated the the lowest binding energies to further identify the binding site of the complexes interacting the proteins. The lowest binding energies of the complexes with the proteins are given in Table 2, the low binding energies indicate a large binding affinity between the complexes and receptors. The binding of the coplexes with five proteins including Beclin-1, p21, mTOR, FAK and caspase 3 show relatively low docking score binding free energy. The results from the binding free energies revealed that complexes exhibited a high affinity of −10.9 kcal/mol with the Beclin-1 among these proteins. Fig. 6 (caspase: a-c, PARP: d-f) shows the optimal docking site view and their activity pockets (other proteins can be found in the **Fig. S11**, supporting information). The sites

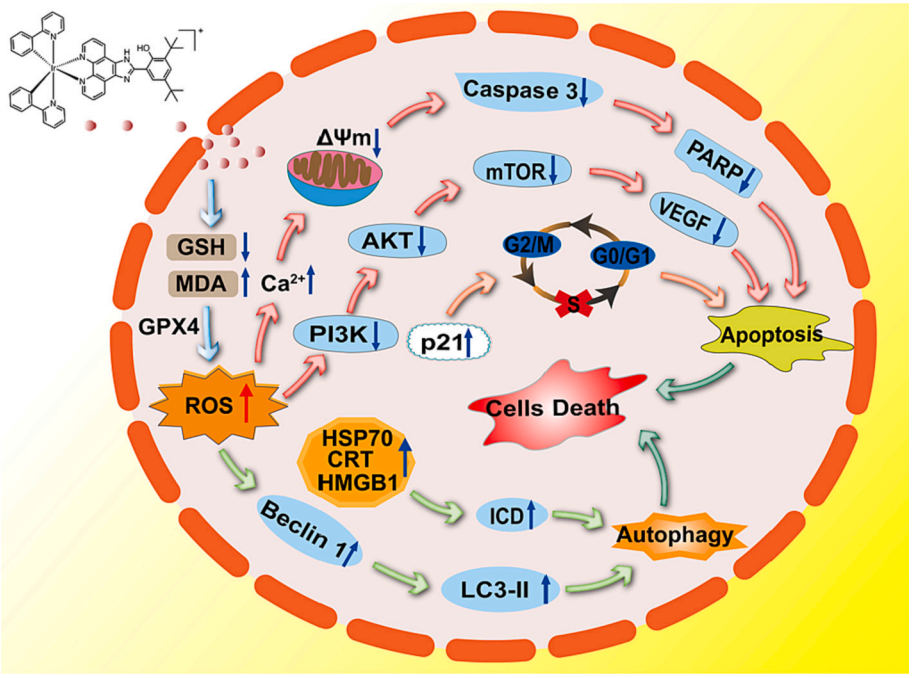

Fig. 7. Apoptotic and autophagy mechanism induced by the complexes **Ir1** and **Ir2**.

where **Ir1** and **Ir2** form hydrogen bonds and interact with residues with amino acids of different proteins are given in **Table S1** (supporting information). Thus, the docking energies were consistent with the western blot results, which may further confirm the regulatory effects of PI3K/AKT/ mTOR in the **Ir1** and **Ir2** treatment progression.

4. Conclusions

In summary, we designed, synthesized, and characterized two new Ir (III) complexes **Ir1** and **Ir2**. MTT results showed that **Ir1** exhibited moderate and **Ir2** showed high cytotoxic activity against tumor cells BEL-7402. These complexes were able to be taken up by BEL-7402 cells, the complexes caused a significant decrease in GSH activity, and an accumulation of toxic epoxidized lipid MDA levels, which then led to an increase of reactive oxygen species and intracellular calcium ion levels. In addition, the complexes caused a decrease in mitochondrial membrane potential and downregulated the expression of caspase 3 and PARP proteins. Meanwhile, the complexes down-regulated PI3K, AKT, VEGF and mTOR proteins, which confirmed that the complexes could induce apoptosis through the pathway of a ROS-mediated mitochondrial dysfunction. The complexes promoted the expression of p21 and blocked the cell cycle at the S phase. On the other hand, we found that complexes can induce autophagy through enhancing the expression of Beclin-1 protein, prompting the transformation of LC3 from LC3-I to LC3-II. We also discovered that the complexes were able to inhibit cell migration and colony formation, decreased the activity of associated protein FAK. Taken together, it has been suggested that the complexes activated the PI3K/AKT/mTOR pathway, which triggered the activation of the Bcl-2 family, thereby inducing apoptosis and autophagy (Fig. 7). Therefore, we can conclude that the complexes may be potent anticancer candidate drugs for the treatment of BEL-7402 cancer.

Declaration of Competing Interest

The authors declare that no competing interests exist.

Data availability

Data will be made available on request.

Acknowledgements

This work was supported by the National Natural Science Foundation of China (No 21877018).

Appendix A. Supplementary data

Supplementary data to this article can be found online at https://doi.org/10.1016/j.jinorgbio.2023.112145.

References

[1] J.M. Llovet, R.K. Kelley, A. Villanueva, A.G. Singal, E. Pikarsky, S. Roayaie, R. Lencioni, K. Koike, J. Zucman-Rossi, R.S. Finn, Hepatocellular carcinoma, Nat. Rev. Dis. Primers. 7 (2021) 6.
[2] R.L. Siegel, K.D. Miller, H.E. Fuchs, A. Jemal, Cancer statistics, 2022, CA Cancer J. Clin. 72 (2022) 7–33.
[3] B. Rodenak-Kladniew, A. Castro, P. Stärkel, M. Galle, R. Crespo, 1,8-cineole promotes G0/G1 cell cycle arrest and oxidative stress-induced senescence in HepG2 cells and sensitizes cells to anti-senescence drugs, Life Sci. 243 (2020), 117271.
[4] H. Zhang, Y.P. Tan, L. Zhao, L. Wang, N.J. Fu, S.P. Zheng, X.F. Shen, Anticancer activity of dietary xanthone α-mangostin against hepatocellular carcinoma by inhibition of STAT3 signaling via stabilization of SHP1, Cell Death Dis. 11 (2020) 63.
[5] R.R. Ye, W. Peng, B.C. Chen, N. Jiang, X.Q. Chen, Z.W. Mao, R.T. Li, Mitochondria-targeted artesunate conjugated cyclometalated iridium(III) complexes as potent anti-HepG2 hepatocellular carcinoma agents, Metallomics 12 (2020) 1131–1141.
[6] C. Huang, C. Liang, T. Sadhukhan, S. Banerjee, Z.X. Fan, T.X. Li, Z.L. Zhu, P. Y. Zhang, K. Raghavachari, H.Y. Huang, In-vitro and in-vivo photocatalytic cancer therapy with biocompatible iridium(III) photocatalysts, Angew. Chem. Int. Ed. 60 (2021) 9474–9479.
[7] L.L. Wang, R.L. Guan, L.N. Xie, X.X. Liao, K. Xiong, T.W. Rees, Y. Chen, L.N. Ji, H. Chao, An ER-targeting iridium(III) complex that induces immunogenic cell death in non-small-cell lung cancer, Angew. Chem. Int. Ed. 60 (2021) 4657–4665.
[8] J.J. Conesa, A.C. Carrasco, V. Rodríguez-Fanjul, Y. Yang, J.L. Carrascosa, P. Cloetens, E. Pereiro, A.M. Pizarro, Unambiguous intracellular localization and quantification of a potent iridium anticancer compound by correlative 3D cryo x-ray imaging, Angew Chem. Int. Ed. Engl. 59 (2020) 1270–1278.
[9] W.W. Qin, Z.Y. Pan, D.H. Cai, Y. Li, L. He, Cyclometalated iridium(III) complexes for mitochondria-targeted combined chemo-photodynamic therapy, Dalton Trans. 49 (2020) 3562–3569.

[10] W.Y. Zhang, S. Banerjee, G.M. Hughes, H.E. Bridgewater, J.I. Song, B.G. Breeze, G. J. Clarkson, J.P.C. Coverdale, C. Sanchez-Cano, F. Ponte, E. Sicilia, P.J. Sadler, Ligand-centred redox activation of inert organoiridium anticancer catalysts, Chem. Sci. 11 (2020) 5466–5480.

[11] J.J. Cao, C.P. Tan, M.H. Chen, N. Wu, D.Y. Yao, X.G. Liu, L.N. Ji, Z.W. Mao, Targeting cancer cell metabolism with mitochondria-immobilized phosphorescent cyclometalated iridium(III) complexes, Chem. Sci. 8 (2017) 631–640.

[12] S.J. Thomas, B. Balónová, J. Jr, M.N. Cinatl, C.J. Wass, B.A. Blight Serpell, M. Michaelis, Thiourea and guanidine compounds and their iridium complexes in drug-resistant cancer cell lines: structure-activity relationships and direct luminescent imaging, ChemMedChem 15 (2020) 349–353.

[13] B.B. Chen, N.L. Pan, J.X. Liao, M.Y. Huang, D.C. Jiang, J.J. Wang, H.J. Qiu, J. X. Chen, L. Li, J. Sun, Cyclometalated iridium(III) complexes as mitochondria-targeted anticancer and antibacterial agents to induce both autophagy and apoptosis, J. Inorg. Biochem. 219 (2021), 111450.

[14] C.H. Lee, Y.L. Shih, M.H. Lee, M.K. Au, Y.L. Chen, H.F. Lu, J.G. Chung, Bufalin induces apoptosis of human osteosarcoma U2OS cells through endoplasmic reticulum stress, caspase- and mitochondria-dependent signaling pathways, Molecules 22 (2017) 437.

[15] E.A. Slee, M.T. Harte, R.M. Kluck, B.B. Wolf, C.A. Casiano, D.D. Newmeyer, H. G. Wang, J.C. Reed, D.W. Nicholson, E.S. Alnemri, D.R. Green, S.J. Martin, Ordering the cytochrome c–initiated caspase cascade: hierarchical activation of caspases-2, −3, −6, −7, −8, and −10 in a caspase-9–dependent manner, J. Cell Biol. 144 (1999) 281–292.

[16] C. Huang, C. Liang, T. Sadhukhan, S. Banerjee, Z. Fan, T. Li, Z. Zhu, P. Zhang, K. Raghavachari, H. Huang, In-vitro and in-vivo photocatalytic cancer therapy with biocompatible iridium(III) photocatalysts, Angew. Chem. Int. Ed. 60 (2021) 9474–9479.

[17] G. Liu, F. Pei, F. Yang, L. Li, A.D. Amin, S. Liu, J. Buchan, W.C. Cho, Role of autophagy and apoptosis in non-small-cell lung Cancer, Int. J. Mol. Sci. 18 (2017) 367.

[18] X.X. Liang, L. Zhang, F.L. Li, S.X. Luan, C.L. He, L.Z. Yin, Z.Q. Yin, Y.F. Zou, G. Z. Yue, L.X. Li, X. Song, C. Lv, W. Zhang, B. Jing, Autophagy-regulating N-heterocycles derivatives as potential anticancer agents. Future, Med. Chem. 12 (2020) 223–242.

[19] Q.Y. Yi, D. Wan, B. Tang, Y.J. Wang, W.Y. Zhang, F. Du, M. He, Y.J. Liu, Synthesis, characterization and anticancer activity in vitro and in vivo evaluation of an iridium (III) polypyridyl complex, Eur. J. Med. Chem. 145 (2018) 338–349.

[20] B.J. Han, G.B. Jiang, J. Wang, W. Li, H.L. Huang, Y.J. Liu, The studies on bioactivity in vitro of ruthenium(II) polypyridyl complexes towards human lung carcinoma A549 cells, RSC Adv. 4 (2014) 40899–40906.

[21] Y.J. Liu, C.H. Zeng, Z.H. Liang, J.H. Yao, H.L. Huang, Z.Z. Li, F.H. Wu, Synthesis of ruthenium(II) complexes and characterization of their cytotoxicity in vitro, apoptosis, DNA-binding and antioxidant activity, Eur. J. Med. Chem. 45 (2010) 3087–3095.

[22] T. Mosmann, Rapid colorimetric assay for cellular growth and survival: application to proliferation and cytotoxicity assays, J. Immunol. Methods 65 (1983) 55–63.

[23] F. Lachaud, A. Quaranta, Y. Pellegrin, P. Dorlet, M.F. Charlot, S. Un, W. Leibl, A. Aukauloo, A biomimetic model of the electron transfer between P680 and the TyrZ-His190 pair of PSII, Angew. Chem. Int. Ed. 44 (2005) 1536–1540.

[24] G.A. Crosby, J.N. Demas, The measurement of photoluminescence quantum yields: a review, J. Phys. Chem. 75 (1971) 991–1024.

[25] E. Zafon, I. Echevarria, S. Barrabes, B.R. Manzano, F.A. Jalon, A.M. Rodriguez, A. Massaguer, G. Espino, Photodynamic therapy with mitochondria-targeted biscyclometallated Ir(III) complexes, multi-action mechanism and strong influence of the cyclometallating ligand, Dalton Trans. 51 (2021) 111–128.

[26] J. Hao, H.M. Liu, J.W. Wang, X.Z. Wang, C.X. Huang, L.J. Liang, J. Chen, Y.J. Liu, Iridium(III) complexes induce cervical carcinoma apoptosis via disturbing cellular redox homeostasis disorder and inhibiting PI3K/AKT/ mTOR pathway, J. Inorg. Biochem. 235 (2022), 111946.

[27] W.L. Li, X.Y. Wu, H.M. Liu, C.L. Shi, Y.H. Yuan, L. Bai, X.F. Liao, Y.Y. Zhang, Y. J. Liu, Enhanced in vitro cytotoxicity and antitumor activity in vivo of iridium(III) complexes liposomes targeting endoplasmic reticulum and mitochondria, J. Inorg. Biochem. 233 (2022), 111868.

[28] Z.Z. Tian, Y.L. Yang, L.H. Guo, G.S. Zhong, J.J. Li, Z. Liu, Dual-functional cyclometalated iridium imine NHC complexes: highly potent anticancer and antimetastatic agents, Inorg. Chem. Front. 5 (2018) 3106–3112.

[29] J.S. Chen, X.H. Huang, Q. Wang, X.L. Chen, X.H. Fu, H.X. Tan, L.J. Zhang, W. Li, J. Bi, FAK is involved in invasion and metastasis of hepatocellular carcinoma, Clin. Exp. Metastas. 27 (2010) 71–82.

[30] Y. Zhou, L. Bai, L. Tian, L.L. Yang, H.W. Zhang, Y.Y. Zhang, J. Hao, Y.Y. Gu, Y. J. Liu, Iridium(III)-BBIP complexes induce apoptosis via PI3K/AKT/mTOR pathway and inhibit A549 lung tumor growth in vivo, J. Inorg. Biochem. 223 (2021), 111550.

[31] Y. Gu, C.F. Zhu, H. Iwamoto, J.S. Chen, Genistein inhibits invasive potential of human hepatocellular carcinoma by altering cell cycle, apoptosis, and angiogenesis, World J Gastroentero 11 (2005) 6512–6517.

[32] N.N. Kreis, F. Louwen, J. Yuan, The multifaceted p21 (Cip1/Waf1/CDKN1A) in cell differentiation, Migration and Cancer Therapy Cancers (Basel) 11 (2019) 1–23.

[33] B. Hu, H.M. An, K.P. Shen, L. Xu, Q. Du, S. Deng, Y. Wu, Liver Yin deficiency tonifying herbal extract induces apoptosis and cell senescence in bel-7402 human hepatocarcinoma cells, Exp. Ther. Med. 3 (2012) 80–86.

[34] J. Plati, O. Bucur, R. Khosravi-Far, Apoptotic cell signaling in cancer progression and therapy, Integr Biol (Camb). 3 (2011) 279–296.

[35] M.O. Hengartner, The biochemistry of apoptosis, Nature 407 (2000) 770–776.

[36] M.C. Maiuri, E. Zalckvar, A. Kimchi, G. Kroemer, Self-eating and self-killing: crosstalk between autophagy and apoptosis, Nat. Rev. Mol. Cell Bio. 8 (2007) 741–752.

[37] J.C. Martinou, R.J. Youle, Mitochondria in apoptosis: Bcl-2 family members and mitochondrial dynamics, Dev. Cell 21 (2011) 92–101.

[38] Q. Lei, X.Y. Huang, L.J. Zheng, F. Zheng, J. Dong, F. Chen, W.B. Zeng, Biosensors for Caspase-3: from chemical methodologies to biomedical applications, Talanta 240 (2022), 123198.

[39] L.D. Walensky, E. Gavathiotis, BAX unleashed: the biochemical transformation of an inactive cytosolic monomer into a toxic mitochondrial pore, Trends Biochem. Sci. 36 (2011) 642–652.

[40] Z.G. Yuan, S.P. Chen, C.J. Chen, J.W. Chen, C.K. Chen, Q.Z. Dai, C.M. Gao, Y. Y. Jiang, Design, synthesis and biological evaluation of 4-amidobenzimidazole acridine derivatives as dual PARP and topo inhibitors for cancer therapy, Eur. J. Med. Chem. 138 (2017) 1135–1146.

[41] M.H. Chen, F.X. Wang, J.J. Cao, C.P. Tan, L.N. Ji, Z.W. Mao, Light-up mitophagy in live cells with dual-functional theranostic phosphorescent iridium(III) complexes, ACS Appl. Mater. Inter. 9 (2017) 13304–13314.

[42] J. Adler, Quantifying colocalization by correlation: the Pearson correlation coefficient is superior to the mander's overlap coefficient, I, Parmryd, Cytom. Part A 77A (2010) 733–742.

[43] C.Z. Zhang, W.Q. Yan, B. Li, B. Xu, Y. Gong, F.H. Chu, Y.Z. Zhang, Q.L. Yao, P. L. Wang, H.M. Lei, A new ligustrazine derivative-selective cytotoxicity by suppression of NF-κB/p65 and COX-2 expression on human hepatoma cells. Part 3, Int. J. Mol. Sci. 16 (2015) 16401–16413.

[44] H. Okada, T.W. Mak, Pathways of apoptotic and non-apoptotic death in tumour cells, Nat. Rev. Cancer 4 (2004) 592–603.

[45] K. Cosentino, A.J. García-Sáez, Mitochondrial alterations in apoptosis, Chem. Phys. Lipids 181 (2014) 62–75.

[46] D. Wan, B. Tang, Y.J. Wang, B.H. Guo, H. Yin, Q.Y. Yi, Y.J. Liu, Synthesis and anticancer properties of ruthenium(II) complexes as potent apoptosis inducers through mitochondrial disruption, Eur. J. Med. Chem. 139 (2017) 180–190.

[47] B. Tang, D. Wan, S.H. Lai, H.H. Yang, C. Zhang, X.Z. Wang, C.C. Zeng, Y.J. Liu, Design, synthesis and evaluation of anticancer activity of ruthenium (II) polypyridyl complexes, J. Inorg. Biochem. 173 (2017) 93–104.

[48] L. Peng, L. Yu, C. Yong-Le, Brassica juncea polysaccharides induce apoptosis of colorectal cancer cells via mitochondrial- and caspase-dependent apoptosis pathways, Trop. J. Pharm. Res. 20 (2021) 2333–2338.

[49] R.Z. Huang, X.C. Huang, B. Zhang, H.Y. Jia, Z.X. Liao, H.S. Wang, 16-O-caffeoyl-16-hydroxylhexadecanoic acid, a medicinal plant-derived phenylpropanoid, induces apoptosis in human hepatocarcinoma cells through ROS-dependent endoplasmic reticulum stress, Phytomedicine 41 (2018) 33–44.

[50] W.O. Carter, P.K. Narayanan, J.P. Robinson, Intracellular hydrogen peroxide and superoxide anion detection in endothelial cells, J. Leukoc. Biol. 55 (1994) 253–258.

[51] R. Franco, M.I. Panayiotidis, J.A. Cidlowski, Glutathione depletion is necessary for apoptosis in lymphoid cells independent of reactive oxygen species formation, J. Biol. Chem. 282 (2007) 30452–30465.

[52] H. Zahreddine, K.L. Borden, Mechanisms and insights into drug resistance in cancer, Front. Pharmacol. 4 (2013) 28.

[53] S.J. Dougan, A. Habtemariam, S.E. McHale, S. Parsons, P.J. Sadler, Catalytic organometallic anticancer complexes, Proc. Natl. Acad. Sci. U. S. A. 105 (2008) 11628–11633.

[54] S.A. Ahmed Amar, R. Eryilmaz, H. Demir, S. Aykan, C. Demir, Determination of oxidative stress levels and some antioxidant enzyme activities in prostate cancer, Aging Male 22 (2019) 198–206.

[55] M.S. Nafie, A.I. Khodair, H.A.Y. Hassan, N.M.A. El-Fadeal, H.A. Bogari, S.S. Elhady, S.A. Ahmed, Evaluation of 2-thioxoimadazolidin-4-one derivatives as potent anti-cancer agents through apoptosis induction and antioxidant activation: in vitro and in vivo approaches, Molecules 27 (2022) 83.

[56] M. Rasool, A. Malik, M.S. Qureshi, R. Ahmad, A. Manan, M. Asif, M.I. Naseer, P. N. Pushparaj, Development of tumor lysis syndrome (TLS): a potential risk factor in cancer patients receiving anticancer therapy, Bioinformation 10 (2014) 703–707.

[57] Y. Wang, C.H. Xia, Y.X. Lv, C.J. Li, Q.B. Mei, H.M. Li, H.J. Wang, S. Li, Crosstalk influence between P38MAPK and autophagy on mitochondria-mediated apoptosis induced by anti-Fas antibody/actinomycin D in human hepatoma bel-7402 cells, Molecules 22 (2017) 1705.

[58] N. Bhagya, K.R. Chandrashekar, Autophagy and cancer: can tetrandrine be a potent anticancer drug in the near future? Biomed. Pharmacother. 148 (2022), 112727.

[59] V. Aggarwal, H.S. Tuli, A. Varol, F. Thakral, M.B. Yerer, K. Sak, M. Varol, A. Jain, M.A. Khan, G. Sethi, Role of reactive oxygen species in cancer progression: molecular mechanisms and recent advancements, Biomolecules 9 (2019) 735.

[60] M. Rodríguez-Arribas, S.M.S. Yakhine-Diop, R.A. González-Polo, M. Niso-Santano, J.M. Fuentes, Turnover of lipidated LC3 and autophagic cargoes in mammalian, Cells. Method. Enzymol. 587 (2017) 55–70.

[61] J. Wang, J. Wang, L. Li, L. Feng, Y.R. Wang, Z. Wang, N.H. Tan, RA-XII, a bicyclic hexapeptidic glucoside isolated from Rubia yunnanensis Diels, exerts antitumor activity by inhibiting protective autophagy and activating AKT-mTOR pathway in colorectal cancer cells, J. Ethnopharmacol. 266 (2021), 113438.

[62] T. Wei, X.J. Xie, P.L. Cao, Magnoflorine improves sensitivity to doxorubicin (DOX) of breast cancer cells via inducing apoptosis and autophagy through AKT/mTOR and p38 signaling pathways, Biomed. Pharmacother. 121 (2020), 109139.

[63] J. Yuan, Z.N. Lei, X. Wang, F. Zhu, D.B. Chen, Ruthenium complex Λ-WH0402 induces hepatocellular carcinoma LM6 (HCCLM6) cell death by triggering the Beclin-1-dependent autophagy pathway, Metallomics 7 (2015) 896–907.

[64] M. Ogawa, Y. Tomita, Y. Nakamura, M.J. Lee, S. Lee, S. Tomita, T. Nagaya, K. Sato, T. Yamauchi, H. Iwai, A. Kumar, T. Haystead, H. Shroff, P.L. Choyke, J.B. Trepel, H. Kobayashi, Immunogenic cancer cell death selectively induced by near infrared photoimmunotherapy initiates host tumor immunity, Oncotarget 8 (2017) 10425–10436.
[65] K. Hayashi, F. Nikolos, Y.C. Lee, A. Jain, E. Tsouko, H. Gao, A. Kasabyan, H. E. Leung, A. Osipov, S.Y. Jung, A.V. Kurtova, K.S. Chan, Tipping the immunostimulatory and inhibitory DAMP balance to harness immunogenic cell death, Nat. Commun. 11 (2020) 6299.
[66] I. Adkins, J. Fucikova, A.D. Garg, P. Agostinis, R. Špíšek, Physical modalities inducing immunogenic tumor cell death for cancer immunotherapy, OncoImmunology 3 (2014), e968434.
[67] J. Thorburn, H. Horita, J. Redzic, K. Hansen, A.E. Frankel, A. Thorburn, Autophagy regulates selective HMGB1 release in tumor cells that are destined to die, Cell Death & Differ. 16 (2009) 175–183.
[68] A. Ahmed, S.W.G. Tait, Targeting immunogenic cell death in cancer, Mol. Oncol. 14 (2020) 2994–3006.
[69] T.J. Wang, N.X. Dang, G.B. Tang, Z.H. Li, X.J. Li, B.Y. Shi, Z. Xu, L. Li, X.F. Yang, C. R. Xu, K. Ye, Integrating bulk and single-cell RNA sequencing reveals cellular heterogeneity and immune infiltration in hepatocellular carcinoma, Mol. Oncol. 16 (2022) 2195–2213.
[70] S.W. Shen, R. Wang, H. Qiu, C. Li, J.H. Wang, J.L. Xue, Q.H. Tang, Development of an autophagy-based and stemness-correlated prognostic model for hepatocellular carcinoma using bulk and single-cell RNA-sequencing, Front. Cell Dev. Biol. 9 (2021), 743910.
[71] G. Ferrín, M. Guerrero, V. Amado, M. Rodríguez-Perálvarez, M. De la Mata, Activation of mTOR signaling pathway in hepatocellular carcinoma, Int. J. Mol. Sci. 21 (2020) 1266.
[72] N. Wu, T.H. Yuan, Z.X. Yin, X.T. Yuan, J.F. Sun, Z.Q. Wu, Q.L. Zhang, C. Redshaw, S.G. Yang, X.T. Dai, Network pharmacology and molecular docking study of the Chinese miao medicine sidaxue in the treatment of rheumatoid arthritis, Drug Des. Devel. Ther. 16 (2022) 435–466.
[73] Y.C. Zhang, H. Cheng, W.K. Li, H. Wu, Y. Yang, Highly-expressed P2X7 receptor promotes growth and metastasis of human HOS/MNNG osteosarcoma cells via PI3K/Akt/GSK3β/β-catenin and mTOR/HIF1α/VEGF signaling, Int. J. Cancer 145 (2019) 1068–1082.